Comput Mech (2013) 51:171–185
DOI 10.1007/s00466-012-0712-z

ORIGINAL PAPER

SUPG and discontinuity-capturing methods for coupled fluid mechanics and electrochemical transport problems

Pablo A. Kler · Lisandro D. Dalcin · Rodrigo R. Paz · Tayfun E. Tezduyar

Received: 21 February 2012 / Accepted: 5 April 2012 / Published online: 21 April 2012

Abstract Electrophoresis is the motion of charged particles relative to the surrounding liquid under the influence of an external electric field. This electrochemical transport process is used in many scientific and technological areas to separate chemical species. Modeling and simulation of electrophoretic transport enables a better understanding of the physicochemical processes developed during the electrophoretic separations and the optimization of various parameters of the electrophoresis devices and their performance. Electrophoretic transport is a multiphysics and multiscale problem. Mass transport, fluid mechanics, electric problems, and their interactions have to be solved in domains with length scales ranging from nanometers to centimeters. We use a finite element method for the computations. Without proper numerical stabilization, computation of coupled fluid mechanics, electrophoretic transport, and electric problems would suffer from spurious oscillations that are related to the high values of the local Péclet and Reynolds numbers and the nonzero divergence of the migration field. To overcome these computational challenges, we propose a stabilized finite element method based on the Streamline-Upwind/Petrov-Galerkin (SUPG) formulation and discontinuity-capturing techniques. To demonstrate the effectiveness of the stabilized formulation, we present test computations with 1D, 2D, and 3D electrophoretic transport problems of technological interest.

Keywords Electrophoresis · Fluid mechanics · Electrochemical transport · Finite element computation · SUPG stabilization · Discontinuity capturing

P. A. Kler (✉)
Central Division of Analytical Chemistry, Forschungszentrum Jülich, Wilhelm-Johnen-Str, 52428 Jülich, Germany
e-mail: p.kler@fz-juelich.de

L. D. Dalcin · R. R. Paz
Centro Internacional de Métodos Computacionales en Ingeniería
Instituto de Desarrollo Tecnológico para la Industria Química,
Universidad Nacional del Litoral—Consejo Nacional de Investigaciones Científicas y Técnicas, Colectora RN 168 Km 472, S3000GLN Santa Fe, Argentina

T. E. Tezduyar
Mechanical Engineering, Rice University, MS 321, 6100 Main Street, Houston, TX 77005, USA

1 Introduction

Electrophoresis is a chemical transport process where charged particles move relative to the surrounding liquid under the influence of an externally applied electric field. The magnitude of the relative velocity depends on the electrophoretic mobility of charged molecules. Electrophoretic mobility is an outcome of the balance between electric and hydrodynamic friction forces, the latter being due to the viscosity of the surrounding solution.

The most common applications of electrophoresis are separation processes. They are based on the separation of molecules due to differences in electrophoretic mobility of ions under an external electric field applied at the ends of capillary tubes, microchannels, or microchambers [39]. Electrophoretic separations comprise a group of different techniques, such as capillary zone electrophoresis, isoelectric focusing, isotachophoresis, free-flow electrophoresis, and capillary electrochromatography [38,64], which are extensively used in chemical and biochemical analysis in many scientific areas, such as genetics, molecular biology, pharmacology, and environment monitoring.

Foundations of electrophoretic separations are in the electrokinetic phenomena that develop when electrolyte solutions interact with charged surfaces. Generally, most substances will acquire a surface electric charge when brought

into contact with an aqueous (polar) medium. The effect of any charged surface (solid walls or molecules in the solution) in an electrolyte solution will be to influence the distribution of nearby ions in the solution. Ions of opposite charge to that surface (counterions) are attracted towards the surface while ions of like charge (coions) are repelled from the surface, leading to the formation of an electric double layer (EDL) [28]. The EDL is a region close to the charged surface where there exists an excess of counterions over coions to neutralize the surface charge. When an external electric field is applied in the axial direction of a channel, as in the case of electrophoretic separation, the electrical forces acting on unbalanced ions drag the surrounding liquid, and electroosmotic flow (EOF) and electrophoresis develop. Consequently, when modeling electrophoretic transport, it is necessary to include the EDL and EOF to have a comprehensive approach. This comprehensive approach has to include the different effects present in the electrophoretic transport, such as diffusion, advection, and reaction, as in the classical transport equation. Moreover, transport due to electric forces must also be considered. This effect is known as migration.

Modeling and simulation of electrophoretic separation is valuable because it can provide a better understanding of the fundamentals of the physical and chemical processes studied. Also, simulation would help with optimizing the device designs and operation parameters, reducing the risk of spending time or money on flawed devices or potentially dangerous experiments.

Early mathematical models of electrophoresis were developed by Saville et al. [43]. These 1D models are valid for monovalent analytes in a stagnant electrolyte solution, without EOF. More complex models of conventional electrophoresis were later reported in [5,22,62]. These models are useful for capillary electrophoresis where the system is inherently 1D due to the uniform section of the capillary and the high aspect ratio. These kind of models can be simulated by using 1D finite differences as is the case in the cited papers. Finite element formulations for electrophoretic transport and 2D computations were presented by Ganjoo and Tezduyar [19] and Ganjoo et al. [20]. That work targeted capillary and free-flow electrophoresis assuming a given velocity field. In the case of electrophoretic separation developed in microfluidic chips, there exist multiple channels with different sections; such systems require more complex domains. Such simulations started with the work of Patankar and Hu [37] and Ermakov et al. [18], using 2D finite element models. Chatterjee [10] developed a 3D finite volume model to study several applications in microfluidics, including isoelectric focusing. Recently, Barz [3] developed a fully coupled model for electrokinetic flow and migration in microfluidic devices employing a 2D finite element model. Other examples of related work are those of Shim et al. [45] and Albrecht et al. [1], using 2D domains and flux corrected transport method.

Numerical simulation of electrophoretic separations in microfluidic chips represents a computationally challenging problem. The large differences between the length scales involved and the multiphysics nature of the problem lead to numerical difficulties, such as multiple nonlinear problems, excessive number of degrees of freedom, and global matrices ill-conditioned because of the high aspect ratios [29]. Therefore, implementations for parallel computing and advanced preconditioning techniques are imperative to achieving accurate numerical results with low computation times. Tsai et al. [63] presented a 2D parallel finite volume algorithm to solve EOF in L-shaped microchannels. Chau et al. [11] reported 3D parallel computation of electrophoretic processes for free-flow electrophoresis using a finite difference method. Kler et al. [31,32] presented finite element simulations for electroosmotic flow, capillary zone electrophoresis, isoelectric focusing, and 2D electrophoresis in 3D complex domains.

It is well known that when solving advection-dominated transport problems, numerical stabilization techniques are needed to avoid spurious oscillations in the solution [8,27]. Generally, these undesirable effects are related to the high values of the nondimensional numbers representing the ratio of the advection to diffusion, such as the local Péclet and Reynolds numbers. Also, in electrophoretic transport problems the strong coupling between the fluid and electric problems generates a nonzero-divergence advection field due to the migration. When the migration field acts on a nonuniform concentration field, it generally results in high gradients or even discontinuities in the concentration of different ions. This requires additional stabilization in the form of discontinuity-capturing (DC) techniques. In addition, a "pressure stabilization" is needed in finite element computation of incompressible flows with equal-order interpolation functions for velocity and pressure.

One of the most popular stabilized finite element formulations for flow and transport problems is the Streamline-Upwind/Petrov-Galerkin (SUPG) formulation. It was introduced for advection–diffusion problems and incompressible flows in [8] and for compressible flows in [27]. The Pressure-Stabilizing/Petrov-Galerkin (PSPG) was introduced in [48,53]. An earlier version of the pressure stabilization, for the Stokes flow, was introduced in [25]. The space–time SUPG/PSPG formulations, as different versions of the Deforming-Spatial-Domain/Stabilized Space–Time (DSD/SST) method, were introduced in [47–49,51,52,58].

Supplementing the SUPG formulation with DC and shock-capturing techniques goes almost as far back as the development of the SUPG formulation. Use of such additional stabilization in the context of advection–diffusion problems and compressible flows was reported in [24,26,55].

The additional stabilization techniques introduced in [55] included the "DRD" stabilization for advection–diffusion–reaction problems with dominant reaction terms. The original DRD stabilization and its newer versions were used extensively in flow and transport problems with dominant reaction or reaction-like terms (see [12–16,35,36,55,56]). Other DC and shock-capturing techniques introduced in conjunction with the SUPG formulation include the Discontinuity-Capturing Directional Dissipation (DCDD) [49] and $YZ\beta$ shock-capturing [50,59], which were also used extensively (see [4,40–42,59–61]).

In the stabilized finite element formulations, an embedded stabilization parameter, which is known as "τ", plays an important role. This stabilization parameter involves a measure of the local length scale (also known as "element length") and other parameters such as the local Reynolds and Courant numbers. Various element lengths and τs were proposed starting with those in [8] and [27], followed by the one introduced in [55]. Various new τ definitions were proposed in recent years, including those with a second, diffusive element length scale [49], those based on the element-level matrices [54], and those based on the element-level vectors [54], which address the difficulties reported at small time step sizes (see [23,54]).

The SUPG formulations for the electrophoretic separation process were reported by Ganjoo and Tezduyar [19] and Ganjoo et al. [20]. Those studies did not have a DC term in the stabilized formulation, and the flow field was assumed to be given. Here we present a stabilized formulation for the coupled fluid mechanics and electrochemical transport problem. The stabilization consists of the SUPG formulation, with suitable τ definitions, and a DC term that is closely related to the DCDD terms proposed in [49,57,59,60].

2 Governing equations

The mathematical model for electrophoretic transport includes the fluid dynamics, electric field, mass transport, chemical reactions, and the coupling of all these.

2.1 Flow field

In the framework of continuum fluid mechanics, fluid velocity $\mathbf{u}$ and pressure p are governed by the Navier–Stokes equations of incompressible flows [33,39]:

$$\rho\left(\frac{\partial \mathbf{u}}{\partial t}+\mathbf{u}\cdot\nabla\mathbf{u}\right)=\nabla\cdot\mathbf{T}+\rho\mathbf{g}+\rho_{\mathrm{el}}\mathbf{E}, \tag{1}$$

$$\nabla\cdot\mathbf{u}=0. \tag{2}$$

Equation (1) represents the conservation of momentum for a Newtonian fluid, where ρ is the density, $\mathbf{g}$ is the gravitational acceleration, $\mathbf{E}$ is the electric field strength, $\mathbf{T}=-p\mathbf{I}+\mu(\nabla\mathbf{u}+\nabla\mathbf{u}^T)$ is the stress tensor, and μ is the viscosity. The last term on the right hand side of Eq. (1) is the contribution of the electrical forces to the momentum balance, where $\rho_{\mathrm{el}}=\mathrm{F}\sum_j z_j c_j$ is the electric charge density of the electrolyte solution, obtained as the summation over all j-type ions, with valence z_j and concentration c_j, and F is the Faraday constant. Equation (2) is the incompressibility constraint.

2.2 Electric field

Charge distribution in an electrolyte solution with solvent permittivity ϵ is related to the electric field $\mathbf{E}$ as

$$\epsilon\nabla\cdot\mathbf{E}=\rho_{\mathrm{el}}, \tag{3}$$

where the electric field is obtained from the associated electric potential Φ as

$$\mathbf{E}=-\nabla\Phi. \tag{4}$$

Modeling electrophoresis problems requires special consideration for the electric field since it involves different contributions in the flow domain, and because it is strongly influenced by the presence of nonuniform electrolyte concentrations. Here, a wall-fitted coordinate system (η,ξ_1,ξ_2) is used, where η is the coordinate normal to the solid boundary, while ξ_1 and ξ_2 are the two orthogonal coordinates tangent to the wall. The first contribution to the electric field comes from the presence of electrostatic charges at the solid–liquid interfaces. The interfacial charge has an associated electric potential ψ that decreases steeply in the η-direction due to the screening produced by counterions and other electrolyte ions in the solution. The value of ψ at the interface [39] depends on the wall–solution interactions and it is known as the electrokinetic potential ζ [7]. There is also a potential ϕ in the flow domain, which arises when a potential difference $\Delta\phi$ is externally applied to drive the electrophoresis and/or induce EOF. As the channel walls are supposed be perfectly insulating, there are no components of the applied electric field normal to the wall. So that, near the walls, ϕ varies only in the ξ_1–ξ_2 plane and the total electric potential Φ can be written as

$$\Phi(\eta,\xi_1,\xi_2)=\psi(\eta)+\phi(\xi_1,\xi_2). \tag{5}$$

This superposition is valid if the applied electric field is small compared to the EDL electric field, as often happens in practice. Introducing the electric potential into Eq. (3) leads to the following equation for the electric potential referred in the wall-fitted coordinate system:

$$\frac{\partial^2\psi}{\partial\eta^2}+\sum_{i=1}^{2}\frac{\partial^2\phi}{\partial\xi_i^2}=-\frac{\rho_{\mathrm{el}}}{\epsilon}. \tag{6}$$

The second term on the left hand side of Eq. (6) is non-zero in electrophoresis problems because the concentration gradients in the fluid induce variations on $\frac{\partial \phi}{\partial \xi_i}$ inside the channel. However, $\frac{\partial^2 \phi}{\partial \xi_i^2}$ are several orders of magnitude smaller than $\frac{\partial^2 \psi}{\partial \eta^2}$ (see also [17,34,46]), which allows splitting the computation of the electric field into two parts as explained below.

2.2.1 Electric double layer

According to the previous analysis, the EDL potential is governed by

$$\frac{\partial^2 \psi}{\partial \eta^2} = -\frac{\rho_{\mathrm{el}}}{\epsilon}. \tag{7}$$

Nevertheless, computational requirements are very large when an entire electrophoretic device is modeled. In that sense, we simplify the computation of the EOF by introducing the so-called thin EDL approximation [6,9], where the EOF is regarded as an electrically induced slip velocity (electroosmotic velocity, $\mathbf{u}_{eo}$) in the direction of the applied electric field. This velocity is determined by the Helmholtz–Smoluchowski equation:

$$\mathbf{u}_{eo} = -\frac{\epsilon \zeta \mathbf{E}}{\mu}. \tag{8}$$

This approximation also implies that $\rho_{\mathrm{el}} \approx 0$ in the fluid outside the EDL, meaning that the last term on the right-hand side of Eq. (1) is negligible, i.e. $\rho_{el}\mathbf{E} \approx 0$. Thus, the electroosmotic velocity is included in the fluid problem as a boundary condition, reducing significantly the computational demand. The simplification is appropriate considering that $\psi(\eta)$ decreases to zero within 1–10 nm from the wall, while the cross-sectional channel or capillary dimensions are typically 20–200 μm.

2.2.2 Bulk fluid

Based on the considerations above, the electric potential ϕ has to be computed using the charge conservation equation in steady state [39]:

$$\nabla \cdot \left(-\sigma \nabla \phi - \mathrm{F} \sum_{j=1}^{N} z_j D_j \nabla c_j + \rho_{\mathrm{el}} \mathbf{u} \right) = 0, \tag{9}$$

where D_j is the diffusion coefficient for the species j, N is the number of different species present in the electrolyte solution, and σ is the electrical conductivity:

$$\sigma = \mathrm{F} \sum_{j=1}^{N} {z_j}^2 \Omega_j c_j. \tag{10}$$

Here Ω_j is the ionic mobility. The terms in parenthesis in Eq. (9) represent the electric current density i, which accounts for the ion fluxes due to flow advection, electrical forces, and diffusion. We note that Eq. (9) reduces to $\nabla^2 \phi = 0$ (i.e., the Laplace's equation for the applied potential), which has historically been used for electric potential calculations, only if the electrolyte concentration and mobility are perfectly uniform and stagnant.

2.3 Mass transport and chemistry

The mass transport of weakly concentrated sample molecules and buffer electrolyte components can be modeled by a linear superposition of the migrative, advective, and diffusive transport mechanisms, plus a source term due to the chemical reactions. In a non-stationary mode, the concentration of each j-type species is governed by [39]

$$\frac{\partial c_j}{\partial t} + \nabla \cdot (-z_j \Omega_j \nabla \phi c_j + \mathbf{u} c_j - D_j \nabla c_j) - r_j = 0, \tag{11}$$

where r_j is the reaction term. Different electrolytes (acids, bases, and ampholytes), analytes, and particularly the hydrogen ion have to be considered. In electrolyte chemistry the processes of association and dissociation are much faster than the transport processes, hence, adopting chemical equilibrium constants to model the reactions of weak electrolytes is a suitable approximation [2]. The strong electrolytes are considered as completely dissociated. Expressions for r_j in modeling the different reactive phenomena and their approximations require a detailed explanation that exceeds the scope of the present work. Some of the most common expressions are presented in the Appendix, and a more complete description can be found in [30].

3 Finite element formulation

In this section we first present the finite element formulations for the fluid mechanics, charge conservation, and mass transport. Following that, the coupling of these equations is described.

3.1 Navier–Stokes equations of incompressible flows

We use the SUPG/PSPG formulation [48,53] of Eqs. (1) and (2). Considering a computational domain Ω with boundary Γ divided into n_{el} finite elements Ω^e, $e = 1, \ldots, n_{\mathrm{el}}$, $\mathcal{E}$ is the set of those elements and H^{1h} is the finite-dimensional space defined as

$$H^{1h} = \left\{ \theta^h | \theta^h \in C^0(\overline{\Omega}), \theta^h|_{\Omega^e} \in P^1, \forall \Omega^e \in \mathcal{E} \right\}, \tag{12}$$

with P^1 representing the first-degree polynomials. The function spaces for the trial and test functions are defined as

$$\begin{aligned} S_{\mathbf{u}}^h &= \{\,\mathbf{u}^h | \mathbf{u}^h \in (H^{1h})^{n_{\mathrm{sd}}}, \mathbf{u}^h \doteq \mathbf{D} \ \text{ on } \Gamma_{\mathbf{D}}\,\}, \\ V_{\mathbf{u}}^h &= \{\,\mathbf{w}^h | \mathbf{w}^h \in (H^{1h})^{n_{\mathrm{sd}}}, \mathbf{w}^h \doteq \mathbf{0} \ \text{ on } \Gamma_{\mathbf{D}}\,\}, \\ S_p^h &= \{\,q | q \in H^{1h}\,\}, \end{aligned} \tag{13}$$

where n_{sd} is the number of space dimensions. It is assumed that both Dirichlet- and Neumann-type boundary conditions could be imposed at different segments of the boundary Γ:

$$\begin{aligned} &\mathbf{u}^h = \mathbf{D} \quad \text{on } \Gamma_{\mathbf{D}}, \\ &\mathbf{n} \cdot \mathbf{T}^h = \mathbf{h} \quad \text{on } \Gamma_{\mathbf{h}}, \end{aligned} \tag{14}$$

where $\Gamma_{\mathbf{D}}$ and $\Gamma_{\mathbf{h}}$ are the complementary subsets of Γ, and $\mathbf{u}^h$ includes the electroosmotic velocity $\mathbf{u}_{eo}$, given by Eq. (8).

The SUPG/PSPG formulation is written as follows: find $\mathbf{u}^h \in S_{\mathbf{u}}^h$ and $p^h \in S_p^h$, such that $\forall \mathbf{w}^h \in V_{\mathbf{u}}^h, \forall q^h \in S_p^h$:

$$\begin{aligned} &\int_\Omega \mathbf{w}^h \cdot \rho\Big(\frac{\partial \mathbf{u}^h}{\partial t} + \mathbf{u}^h \cdot \nabla \mathbf{u}^h\Big) d\Omega \\ &\quad + \int_\Omega \nabla \mathbf{w}^h : \mathbf{T}^h d\Omega - \int_\Omega \mathbf{w}^h \cdot \Big(\rho \mathbf{g} + \rho_{\mathrm{el}}^h \mathbf{E}\Big) d\Omega \\ &\quad + \sum_{e=1}^{n_{\mathrm{el}}} \int_{\Omega^e} \Big(\tau_{\mathrm{SUPG}} \mathbf{u}^h \cdot \nabla \mathbf{w}^h + \tau_{\mathrm{PSPG}} \frac{1}{\rho} \nabla q^h\Big) \\ &\quad \cdot \Big[\rho\Big(\frac{\partial \mathbf{u}^h}{\partial t} + \mathbf{u}^h \cdot \nabla \mathbf{u}^h\Big) - \nabla \cdot \mathbf{T}^h - \rho \mathbf{g} - \rho_{\mathrm{el}}^h \mathbf{E}\Big] d\Omega \\ &\quad + \int_\Omega q^h \nabla \cdot \mathbf{u}^h \, d\Omega = \int_{\Gamma_{\mathbf{h}}} \mathbf{w}^h \cdot \mathbf{h} \, d\Gamma \end{aligned} \tag{15}$$

The stabilization parameters in Eq. (15) are defined as

$$\begin{aligned} \tau_{\mathrm{SUPG}} &= \tau_{\mathrm{PSPG}} = \left(\frac{1}{\tau_1^2} + \frac{1}{\tau_2^2} + \frac{1}{\tau_3^2}\right)^{-\frac{1}{2}}, \\ \tau_1 &= \frac{h_{\mathrm{SUPG}}}{2||\mathbf{u}^h||}, \\ \tau_2 &= \frac{\Delta t_{\mathrm{NS}}}{2}, \\ \tau_3 &= \rho \frac{h_{\mathrm{SUPG}}^2}{12\mu}. \end{aligned} \tag{16}$$

Here, Δt_{NS} is the time step size and the element length h_{SUPG} is defined [55] as

$$h_{\mathrm{SUPG}} = 2||\mathbf{u}^h|| \left(\sum_{a=1}^{n_{\mathrm{en}}} |\mathbf{u}^h \cdot \nabla N_a|\right)^{-1}, \tag{17}$$

where n_{en} the number of element nodes and N_a is the interpolation function associated with element node a.

3.2 Electric problem

For the finite element formulation of Eq. (9), the function spaces for the trial and test functions are defined as

$$\begin{aligned} S_\phi^h &= \{\,\phi^h | \phi^h \in H^{1h}, \phi^h \doteq \varphi^h \ \text{ on } \Gamma_\varphi\,\}, \\ V_\phi^h &= \{\,v^h | v^h \in H^{1h}, v^h \doteq 0 \ \text{ on } \Gamma_\varphi\,\}. \end{aligned} \tag{18}$$

It is assumed that only Dirichlet-type boundary conditions are imposed at one or more segments Γ_φ of the boundary Γ:

$$\phi = \varphi \quad \text{on } \Gamma_\varphi. \tag{19}$$

The Galerkin formulation of the problem can be written as follows: find $\phi^h \in S_\phi^h$, such that $\forall v^h \in V_\phi^h$:

$$\begin{aligned} &\int_\Omega \nabla v^h \cdot \sigma^h \nabla \phi^h \, d\Omega \\ &\quad = \int_\Omega \nabla v^h \cdot \left(-\mathrm{F} \sum_{j=1}^{N} z_j D_j \nabla c_j^h + \rho_{\mathrm{el}}^h \mathbf{u}^h\right) d\Omega. \end{aligned} \tag{20}$$

3.3 Mass transport problem

For the finite element formulation of Eq. (11), the function spaces for the trial and test functions are defined as

$$\begin{aligned} S_j^h &= \{\,c_j^h | c_j^h \in H^{1h}, c_j^h \doteq C_j \ \text{ on } \Gamma_{C_j}\,\}, \\ V_j^h &= \{\,v^h | v^h \in H^{1h}, v^h \doteq 0 \ \text{ on } \Gamma_{C_j}\,\}. \end{aligned} \tag{21}$$

It is assumed that both Dirichlet- and Neumann-type boundary conditions could be imposed at different segments of the boundary Γ:

$$\begin{aligned} &c_j^h = C_j \quad \text{on } \Gamma_{C_j}, \\ &\mathbf{n} \cdot \nabla c_j^h = F_j \quad \text{on } \Gamma_{F_j}, \end{aligned} \tag{22}$$

where Γ_{C_j} and Γ_{F_j} are the complementary subsets of Γ.

The SUPG+DC formulation [49,57,59,60] for this problem is given as follows: find $c_j^h \in S_j^h$, such that $\forall v^h \in V_j^h$:

$$\begin{aligned} &\int_\Omega v^h \left[\frac{\partial c_j^h}{\partial t} + \nabla \cdot \left(-z_j \Omega_j^h \nabla \phi^h c_j^h + \mathbf{u}^h c_j^h\right)\right] d\Omega \\ &\quad + \int_\Omega \nabla v^h \cdot D_j \nabla c_j^h \, d\Omega - \int_\Omega v^h r_j \, d\Omega \\ &\quad + \sum_{e=1}^{\mathrm{nel}} \int_{\Omega^e} \tau_{\mathrm{SUPG}\,j} \left(-z_j \Omega_j^h \nabla \phi^h + \mathbf{u}^h\right) \cdot \nabla v^h \\ &\quad \times \left[\frac{\partial c_j^h}{\partial t} + \nabla \cdot \left(-z_j \Omega_j \nabla \phi^h c_j^h + \mathbf{u}^h c_j^h + D_j \nabla c_j^h\right) - r_j\right] d\Omega \end{aligned}$$

$$+\sum_{e=1}^{n_{\text{el}}}\int_{\Omega^e} \nu_{\text{DC}j}\nabla v^h \nabla c_j^h \, d\Omega = \int_{\Gamma_{F_j}} v^h F_j^h d\Gamma. \tag{23}$$

We note that the SUPG stabilization involves the residuals of the governing equations, which include the second-order term $\nabla\cdot(D_j\nabla c_j^h)$. In this case, for linear (triangular and tetrahedral) elements, the term vanishes. For additional details, the reader is referred to [54]. In the case of the second-order term involving $\nabla\cdot(\nabla\phi^h)$, the term is evaluated by treating $(-z_j\Omega_j^h\nabla\phi^h)$ like a (non-incompressible) velocity field, where ϕ^h comes from the solution of Eq. (20).

The stabilization parameter τ_{SUPGj} for each j-species is defined as

$$\begin{aligned}
\tau_{\text{SUPG}j} &= \left(\frac{1}{\tau_{1j}^2}+\frac{1}{\tau_2^2}+\frac{1}{\tau_{3j}^2}+\frac{1}{\tau_{4j}^2}\right)^{-\frac{1}{2}},\\
\tau_{1j} &= \frac{h_{\text{SUPG}j}}{2||-z_j\Omega_j^h\nabla\phi^h+\mathbf{u}^h||},\\
\tau_2 &= \frac{\Delta t_{\text{MT}}}{2},\\
\tau_{3j} &= \frac{h_{\text{SUPG}j}^2}{12D_j},\\
\tau_{4j} &= \frac{1}{\nabla\cdot\left(-z_j\Omega_j^h\nabla\phi^h\right)}.
\end{aligned} \tag{24}$$

Here, Δt_{MT} is the time step size and the element length $h_{\text{SUPG}j}$ for species j is defined [55] as

$$\begin{aligned}
h_{\text{SUPG}j} &= 2||-z_j\Omega_j^h\nabla\phi^h+\mathbf{u}^h||\\
&\times\left(\sum_{a=1}^{n_{\text{en}}}|\left(-z_j\Omega_j^h\nabla\phi^h+\mathbf{u}^h\right)\cdot\nabla N_a|\right)^{-1}.
\end{aligned} \tag{25}$$

The DC parameter ν_{DCj} for species j is defined as

$$\nu_{\text{DC}j} = \frac{h_{\text{DC}j}}{2}||-z_j\Omega_j^h\nabla\phi^h+\mathbf{u}^h||\left(\frac{||\nabla c_j^h||h_{\text{DC}j}}{c_{\text{ref}\,j}}\right)^2, \tag{26}$$

where $c_{\text{ref}\,j}$ is a reference value for the concentration of the j-species, and

$$h_{\text{DC}j} = 2||\nabla c_j^h||\left(\sum_{a=1}^{\text{nen}}|\nabla c_j^h\cdot\nabla N_a|\right)^{-1}. \tag{27}$$

3.4 Coupling

Starting from an initial or previous state of all the fields (electric potential, velocity, pressure, and the concentration of each species), the first unknown to be updated is the electric potential (ϕ^h), using Eq. (20) with the Dirichlet-type boundary condition given in Eq. (19). Next, the new velocity ($\mathbf{u}^h$) and pressure (p^h) are computed by advancing Eq. (15) a single time step Δt_{NS}. As mentioned in Sect. 2.2, we assume in this work that the EDL length is considerably smaller than the channel width.[1] Consequently, we can assume $\rho_{\text{el}}\approx 0$ in the bulk fluid and the electric force term in Eq. (15) vanishes. The electric forces in the EDL are included in the fluid problem as a Dirichlet boundary condition modeled by the Helmholtz–Smoluchowski approximation for the slip velocity given by Eq. (8). To calculate this velocity, the updated electric potential (ϕ^h) is used.

After that, the concentrations of all species (c_j^h, for $j=1\ldots N$) are updated simultaneously by solving Eq. (23), using the updated potential (ϕ^h) and velocity ($\mathbf{u}^h$). The equations are advanced n_{MT} steps using a smaller time step Δt_{MT}:

$$\Delta t_{\text{NS}} = n_{MT}\,\Delta t_{\text{MT}}, \tag{28}$$

where, at each step with Δt_{MT}, linearly-interpolated values of ϕ^h and $\mathbf{u}^h$ are used. The updated concentration field enables the calculation of the new conductivity field using Eq. (10) and the start of a new cycle by updating the electric potential. The process described above is carried out once for each step with Δt_{NS}.

The flow field is treated as quasi-steady because the characteristic time scales for advection and diffusion are considerably larger than the characteristic time scale for reaction. For the same reason, the electric field is steady. Consequently, there exist two time steps that govern the solution of the complete problem. In updating the flow field, the larger time step (Δt_{NS}) is determined to achieve a maximum local Courant number (CFL) close to 1.0:

$$\text{CFL} = \max_{e\in\mathcal{E},\ 1\le j\le N}\left\{\frac{||-z_j\Omega_j^h\nabla\phi^h+\mathbf{u}^h||\Delta t_{\text{NS}}}{h_{\text{SUPG}j}}\right\}. \tag{29}$$

The smaller time step (Δt_{MT}) used in updating the concentration fields is determined by the reaction coefficient that models the fastest reaction.

4 Numerical examples

The first numerical experiment is a 1D simulation of a capillary electrophoresis assay, where we test different stabilization parameters. Following that, a 2D application example with several species and different advection fields acting on the transported sample along different directions is presented. Finally a 3D test where the main flow is split and recombined to obtain an efficient mixing of two buffer components is studied.

[1] For cases where the EDL length is comparable to the channel width, we compute the charge density by using the Poisson–Boltzmann equation and the fluid mechanics problem does include the electric force term; see [30,32] for more details.

Table 1 Physicochemical properties of the buffer components and analytes

Component	pK_a [a]	pK_b	Mobility (m^2/Vs)	Diffusivity (m^2/s)
Hydrochloric acid	−2.0	–	7.91×10^{-8}	2.03×10^{-9}
Tetraphenylborate	5.0	–	1.80×10^{-8}	4.60×10^{-10}
TRIS	–	8.08	2.95×10^{-8}	7.60×10^{-10}
Acetic acid	4.76	–	4.20×10^{-8}	1.08×10^{-9}

[a] pK represents the commonly used notation for equilibrium constants: $pK = -\log_{10} K$

4.1 1D test: capillary electrophoresis

In this first test we demonstrate the effects of using the SUPG and DC stabilizations in advection-dominated problems, specifically in separation by capillary electrophoresis (CE). In a CE assay, an electric potential difference is applied between the ends of a microchannel to obtain a longitudinal electric field. This electric field exerts forces on the charged molecules in the solution, resulting in different electrophoretic velocities and enabling the separation of the sample components. In this example, two acidic species (hydrochloric acid and tetraphenilborate) are separated using a low-concentration buffer of tris(hydroxymethyl)-aminoetane (TRIS) and acetic acid. Physicochemical properties of the buffer and analytes are listed in Table 1. Initial conditions for the samples and buffer components are shown in Fig. 1a. Due to the relatively low concentration of the buffer components, samples and their motion affect the local physicochemical properties of the electrolyte solution. This means that the local presence of the sample in a region of the capillary affects both the electric conductivity and the local acid–base equilibrium (i.e., the pH of the solution), as seen in Fig. 1a. The former affects the local values of the electric field, and the latter alters the effective mobility of the samples (see Eqs. (39) and (40)), producing a strong dual coupling between the numerical solutions of the electric field and the transport equations (Eqs. (9) and (11)). This can be inferred from Fig. 1b. To carry out the test, a 3000 V difference of electric potential is applied between the end walls of a 5 cm long capillary, which is filled with the electrolytic solution. As mentioned earlier, this potential difference generates an electric field that exerts electric forces on the samples, which enables the separation due to the differences in effective mobilities. Due to the local values of pH, hydrochloric acid mobility is higher than the tetraphenilborate one; and consequently the displacement of hydrochloric acid is higher.

Figure 2 shows the sample-concentration distributions at two instants and the effect of the stabilization terms on these solutions. It is clear that the stabilization reduces the spurious oscillations in the numerical solutions.

4.2 2D test: free-flow electrophoresis

In this test we demonstrate the effectiveness of the proposed method in simulating electrophoretic transport with conjugation of the flow advection field and migration field in variable directions. In this case the electrophoretic separation process is simulated by using the free-flow electrophoresis (FFE) method.

The FFE is a continuous technique for electrophoretic separation. These methods provide bands across the separation chamber and thus a continuous supply of separated components at the exit of the chamber. In FFE, sample components are injected into a liquid carrier with an electric field applied perpendicular to the flow direction. Particles are deflected from the flow streamlines at an angle arranged by the vector composition of the flow advection and the migration (determined by the local sample mobility and the electric field strength). Sample components with different electrophoretic

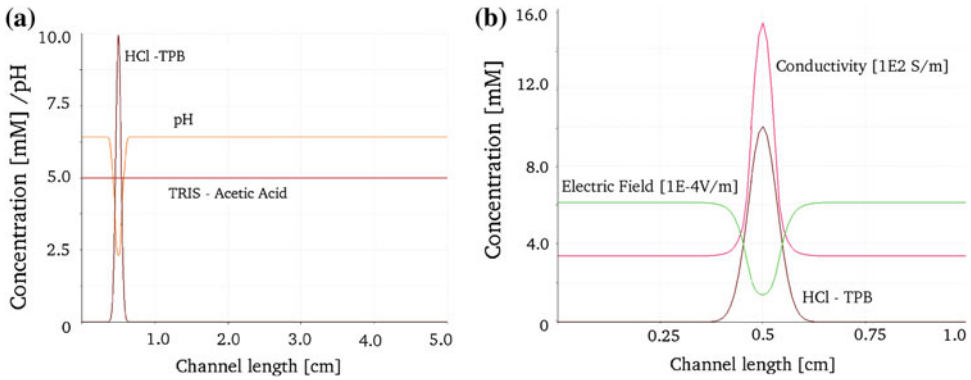

Fig. 1 Initial conditions for the samples, buffer components, conductivity, and electric field. **a** Samples and buffer components. **b** Concentration, conductivity, and electric field coupling

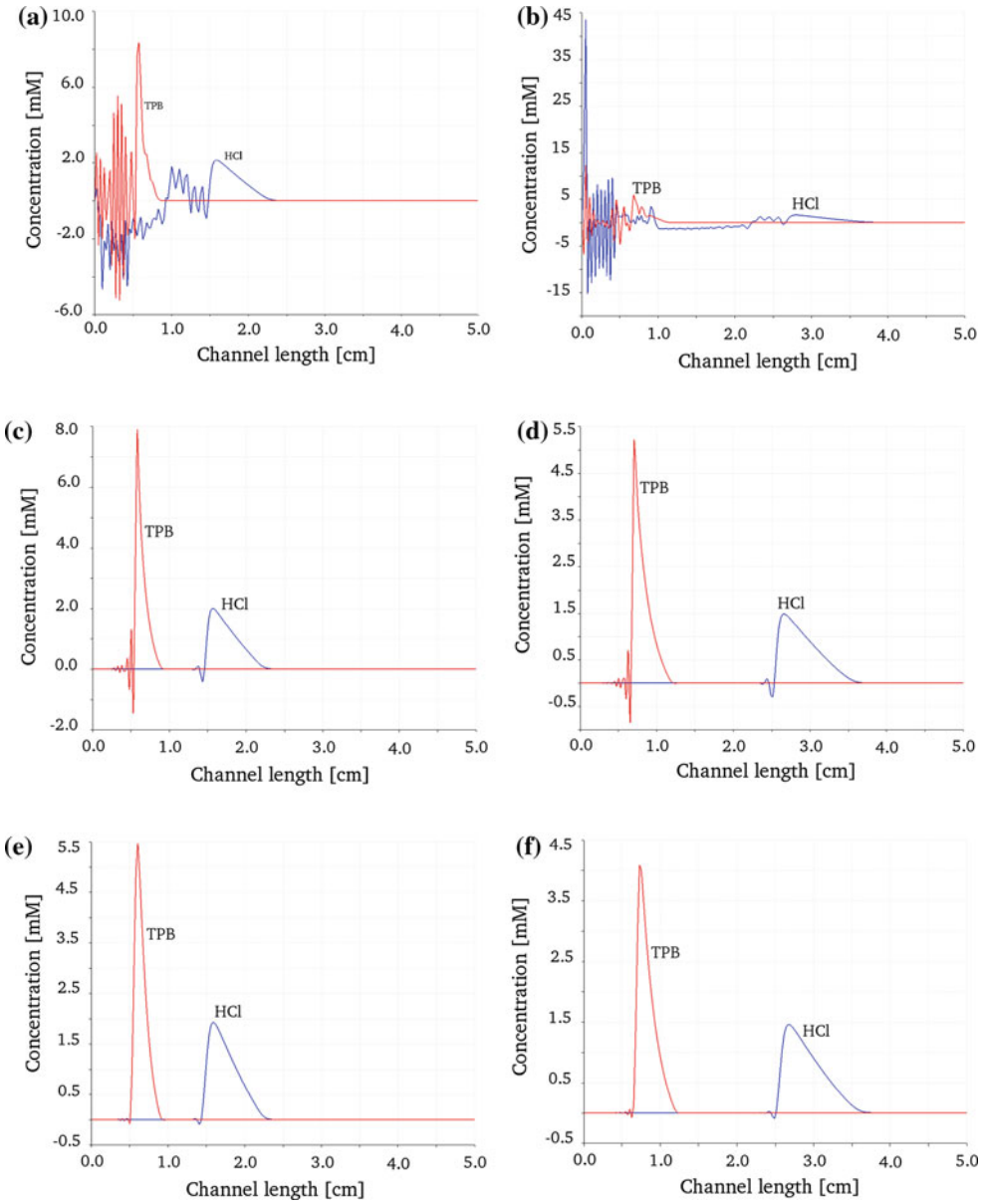

Fig. 2 Sample concentrations for the CE assay at t = 3 s and t = 6 s for different stabilization schemes. **a** Without stabilization, t = 3 s. **b** Without stabilization, t = 6 s. **c** With SUPG, t = 3 s. **d** With SUPG, t = 6 s. **e** With SUPG+DC, t = 3 s. **f** With SUPG+DC, t = 6 s

mobilities have different deflections and can be collected separately at the end of the separation area.

In this example, two aminoacids from a single flow are separated in two streams and redirected to two separate exit channels. Physicochemical properties of the analytes are listed in Table 2.

To develop the FFE, a 750 V electric potential difference is applied at the outlets and the flow field is developed by imposing a velocity of 1.0 cm/s at the inlet and zero pressure at the outlets. The dimensions are $3.0 \times 1.0\,\text{mm}^2$ for the chamber and $1.0 \times 0.1\,\text{mm}^2$ for the channels. Geometry of the FFE device, electric potential, electric field, and field lines are shown in Fig. 3. The pressure field, velocity field, and the streamlines are shown in Fig. 4. The superposition of the migration and advection effects with variable directions can be inferred from the field lines in Fig. 3 and the streamlines in Fig. 4. The resulting motion of the substances will be the superposition of these effects (plus the dispersion due to the diffusion), producing the separation of the aminoacids. Due to the differences in the degree of dissociation, the mobility is negative for the aspartic acid and positive for the lysine, enabling the electrophoretic separation. As a result, the aspartic acid tends to move downwards to the positive potential region and enters the bottom channel, while lysine moves

Table 2 Physicochemical properties of the analytes

Component	pK_a	pK_b	Mobility (m^2/Vs)	Diffusivity (m^2/s)	Initial concentration (mM)
Aspartic acid	2.28	3.90	2.83×10^{-8}	7.31×10^{-9}	1.0
Lysine	9.12	10.79	2.70×10^{-8}	6.98×10^{-10}	1.0

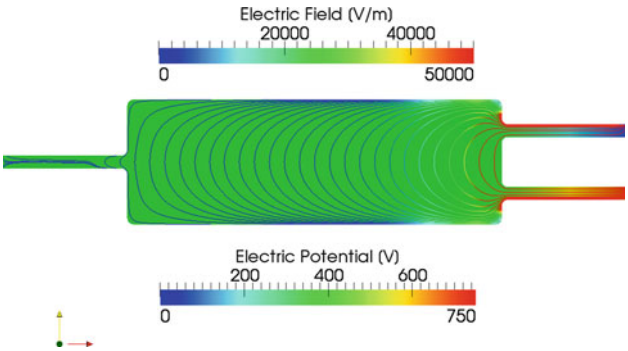

Fig. 3 Electric potential, electric field, and field lines. Electric potential values are represented by the *background colors*, and electric field magnitude by *line colors*. (color figure online)

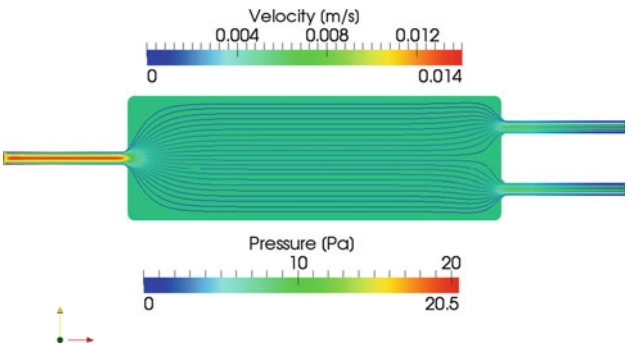

Fig. 4 Pressure, velocity, and streamlines. Pressure values are represented by the *background colors*, and velocity magnitude by *line colors*. (color figure online)

upward, entering the upper channel. Aspartic acid and lysine concentration distributions at different instants are shown in Fig. 5.

Figure 6 shows the concentration distributions for aspartic acid and lysine at the same instants as in Fig. 5, but without the numerical stabilization. It can be seen that the stabilization is essential when the streamlines change direction more rapidly.

4.3 3D application example: split-and-recombine micro-mixer

In this test a split-and-recombine micro-mixer inspired by the earlier work of Schonfeld et al. [44] is simulated to show the capability of the simulation tool developed for solving 3D flow and transport problems. We compare the mixing efficiencies of the pressure driven and EOF driven mixers.

At the microscale, the fluid flow is inherently laminar, and because of that mixing and homogenization of the electrolyte solution results in a challenging problem from a technological point of view [21]. In this example the mixing technique consists of splitting and recombining the flow. First the flow is split into two parts: the upper half and the lower half. Then, these two parts of the flow are recombined horizontally: the upper half fills the left half of exit channel and the lower half fills the right half. This mixing technique is employed to obtain a uniform buffer solution commonly used in electrophoresis assays. The buffer solution is composed of equal parts of acetic acid and TRIS. Physicochemical properties of the buffer components employed in this example can be found in Table 1.

The dimensions of the mixer are $100 \times 40\ \mu m^2$ for the rectangular section at the inlet and outlet, and 4 mm for the length of the device. The geometry and the velocity and pressure fields are shown in Figs. 7 and 8 for the pressure driven and EOF driven mixers, respectively. The pressure driven flow field is obtained by imposing a uniform velocity of 1.0 mm/s at the inlet and zero pressure at the outlet. The EOF driven flow field is obtained by applying an electric potential difference of 50.0 V (based on an electrokinetic potential $\zeta = 0.8$ mV) and zero pressure at the outlet. Concentration distributions for the buffer components and the resulting pH of the solution at different instants are shown in Figs. 9 and 10 for the pressure driven and EOF driven mixing, respectively. We also evaluate the sample distributions and the pH at the outlet cross section to determine which flow type provides a more efficient mixing. Figure 11 shows the concentration and pH profiles at the outlet cross section. From the latter it can be inferred that the plug-like velocity profile of the EOF driven flow is less efficient than the parabolic profile of the pressure driven flow. Also, it is worth mentioning that the efficiency of the EOF mixing decreases due to the influence of the migration terms, speeding up the TRIS and slowing down the acetic acid relative to the fluid flow.

The equilibrium pH for the buffer solution is theoretically determined as 6.42, which is close to the center of the pH range obtained at the outlet by the pressure driven mixing. Also, the pressure driven mixing provides a narrower range

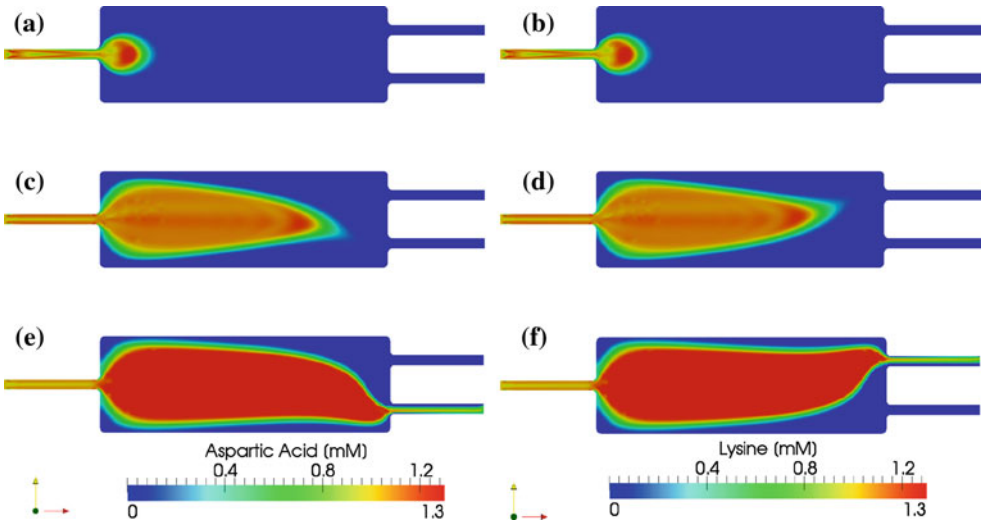

Fig. 5 Aspartic acid (*left*) and lysine (*right*) distributions at different instants. **a** t = 0.25 s. **b** t = 0.25 s. **c** t = 1.75 s. **d** t = 1.75 s. **e** t = 3.0 s. **f** t = 3.0 s

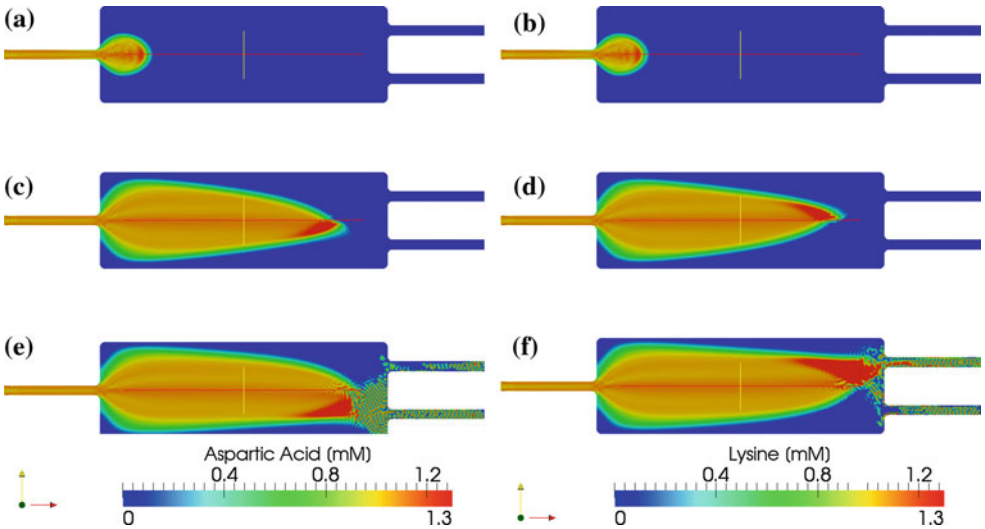

Fig. 6 Aspartic acid (*left*) and lysine (*right*) distributions at different instants, without numerical stabilization. **a** t = 0.25 s. **b** t = 0.25 s. **c** t = 1.75 s. **d** t = 1.75 s. **e** t = 3.0 s. **f** t = 3.0 s

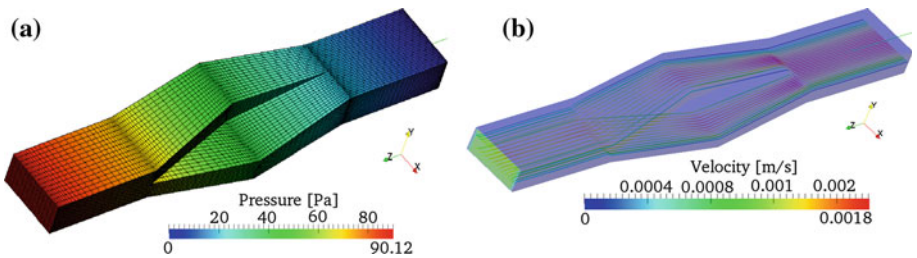

Fig. 7 Pressure, velocity, and streamlines for the pressure driven mixing. The pictures have been scaled by 0.2 in the z-direction to enhance the visualization. **a** Pressure field. **b** Velocity field

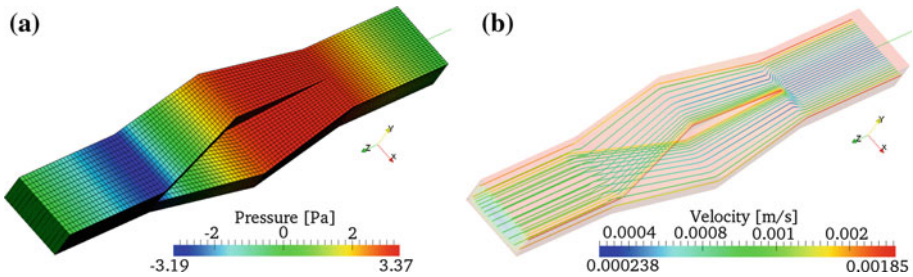

Fig. 8 Pressure, velocity, and streamlines for the EOF driven mixing. The pictures have been scaled by 0.2 in the z-direction to enhance the visualization. **a** Pressure field. **b** Velocity field

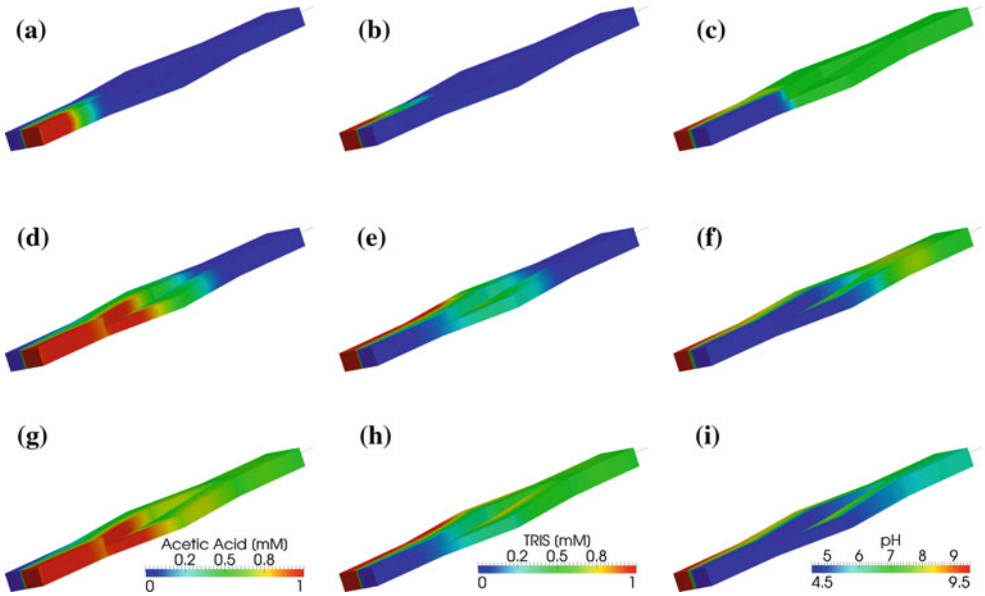

Fig. 9 Acetic acid, TRIS, and pH distributions at different instants for the pressure driven mixing. The pictures have been scaled by 0.2 in the z-direction to enhance the visualization. **a** t = 1.0 s. **b** t = 1.0 s. **c** t = 1.0 s. **d** t = 3.0 s. **e** t = 3.0 s. **f** t = 3.0 s. **g** t = 7.0 s. **h** t = 7.0 s. **i** t = 7.0 s

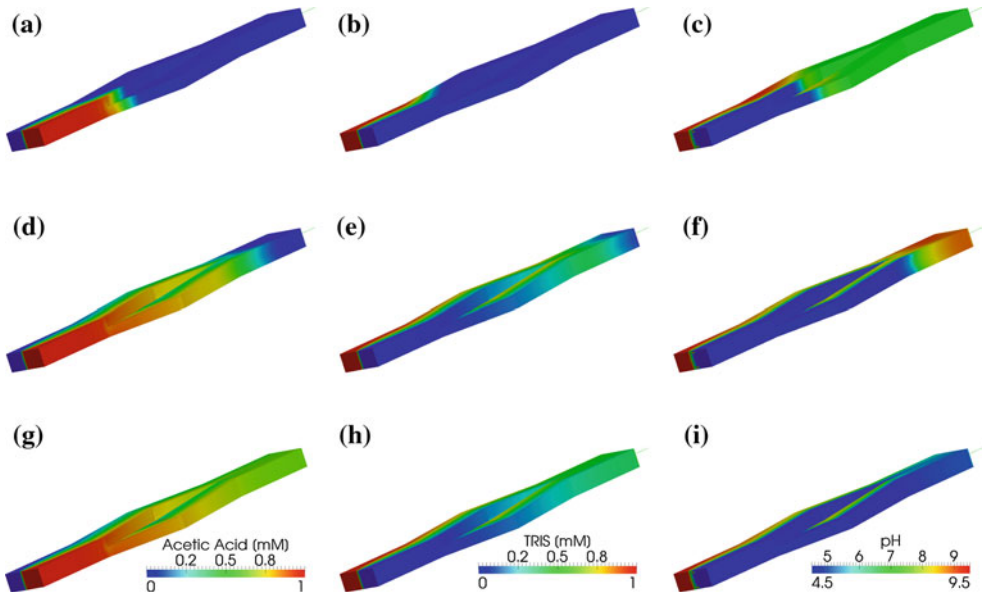

Fig. 10 Acetic acid, TRIS, and pH distributions at different instants for the EOF driven mixing. The pictures have been scaled by 0.2 in the z-direction to enhance the visualization. **a** t = 1.0 s. **b** t = 1.0 s. **c** t = 1.0 s. **d** t = 3.0 s. **e** t = 3.0 s. **f** t = 3.0 s. **g** t = 7.0 s. **h** t = 7.0 s. **i** t = 7.0 s

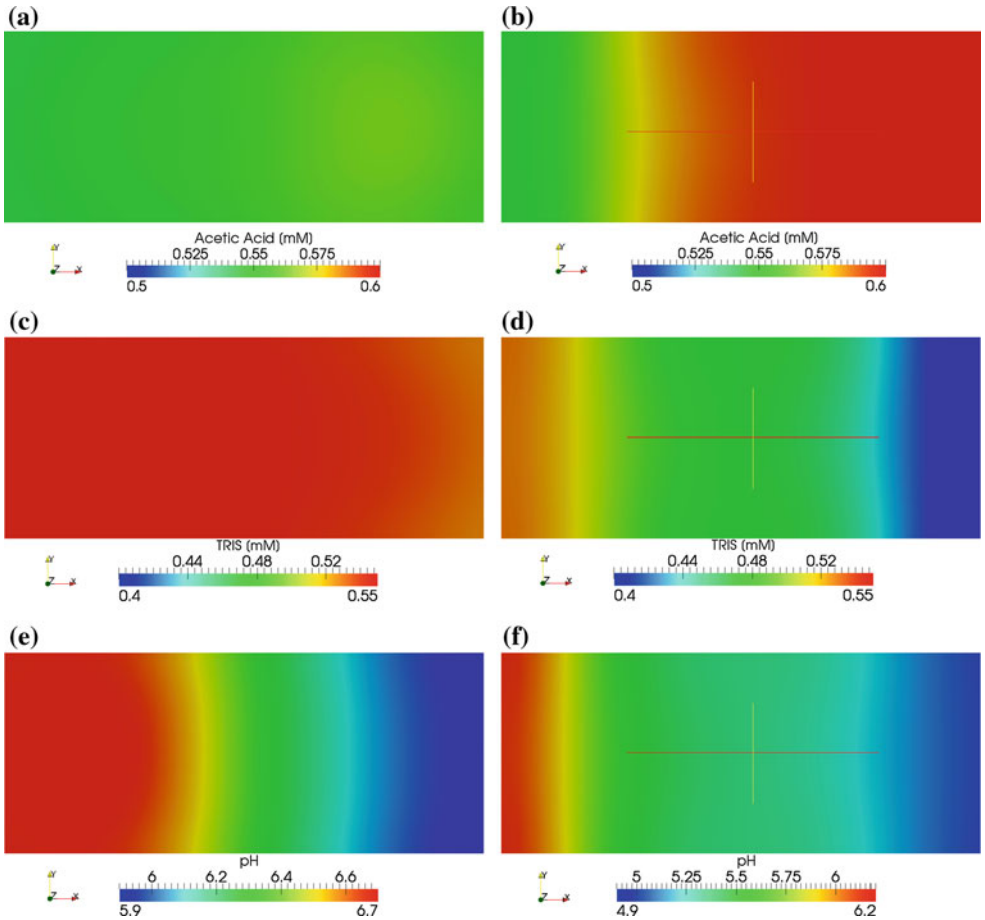

Fig. 11 Acetic acid, TRIS, and pH distributions for a cross section at the outlet of the mixer. **a** Pressure driven. **b** EOF driven. **c** Pressure driven. **d** EOF driven. **e** Pressure driven. **f** EOF driven

of pH (less than 0.7) compared to the EOF driven mixing (≈1.3).

5 Concluding remarks

We presented a stabilized finite element formulation for computing coupled fluid mechanics and electrophoretic transport equations. The formulation is based on the SUPG and DC methods developed for scalar and vector equations. We proposed expressions for the stabilization and DC parameters τ_{SUPG} and ν_{DC}, accounting for the diffusion, advection, and reaction effects associated with the electrophoretic processes.

We presented some test computations and application examples to asses the effectiveness of the formulation. The first example was a 1D capillary electrophoresis problem. The SUPG+DC formulation reduces substantially the spurious oscillations that are typically observed in solution of advection-dominated problems without stabilization. The second example shows a typical application of free-flow electrophoretic separation. In these problems, the fluid velocity and the electric field have variable directions. The SUPG+DC formulation can effectively handle the combination of fluid and electric advection effects. The last example helps us evaluate the mixing performance of a 3D micromixer under different flow conditions. The complexity of this example demonstrate that the proposed formulation is suitable for solving electrophoretic problems for a wide range of applications.

With the advent of more complex microfluidic devices, classical 1D models for electrophoresis is no longer suitable to represent both physicochemical phenomena and design characteristics. Consequently, more complex simulation frameworks are needed for design and optimization. This work contributes to the enhancement of finite element simulations in the emerging technology of microfluidic chips.

Acknowledgments This work has received financial support from *Consejo Nacional de Investigaciones Científicas y Técnicas* (CONICET, Argentina, grant PIP 5271/05), *Universidad Nacional del Litoral* (UNL, Argentina, grant CAI+D 2009 65/334 and 65/238), *Agencia Nacional de Promoción Científica y Tecnológica* (ANPCyT, Argentina, grants PICT 01141/2007, PICT 0270/2008, PICT-1506/2006).

Appendix

Acid–base reactions

For the general case, reactions associated with an ampholyte AH with concentration c_{AH} are

$$\mathrm{AH} \underset{k_{a2}}{\overset{k_{a1}}{\rightleftharpoons}} \mathrm{A}^- + \mathrm{H}^+, \tag{30}$$

$$\mathrm{AH}_2^+ \underset{k_{b2}}{\overset{k_{b1}}{\rightleftharpoons}} \mathrm{AH} + \mathrm{H}^+, \tag{31}$$

where k_{a1} and k_{b1} are the dissociation rates and k_{a2} and k_{b2} are the association rates for the acidic and basic reactions, respectively. Then the equilibrium state is characterized by

$$\frac{k_{a2}}{k_{a1}} = \frac{c_{\mathrm{A}^-}\, c_{\mathrm{H}^+}}{c_{\mathrm{AH}}} = K_a, \tag{32}$$

$$\frac{k_{b2}}{k_{b1}} = \frac{c_{\mathrm{AH}}\, c_{\mathrm{H}^+}}{c_{\mathrm{AH}_2^+}} = K_b, \tag{33}$$

where K_a and K_b are the equilibrium constants for the acidic and basic reactions, respectively. The corresponding expressions for r_j are obtained as follows:

$$r_{\mathrm{A}^-} = -k_{a1}\, c_{\mathrm{A}^-}\, c_{\mathrm{H}^+} + k_{a2}\, c_{\mathrm{AH}}, \tag{34}$$

$$r_{\mathrm{AH}} = k_{a1}\, c_{\mathrm{A}^-}\, c_{\mathrm{H}^+} - k_{a2}\, c_{\mathrm{AH}} - k_{b1}\, c_{\mathrm{AH}}\, c_{\mathrm{H}^+} + k_{b2}\, c_{\mathrm{AH}_2^+}, \tag{35}$$

$$r_{\mathrm{AH}_2^+} = k_{b1}\, c_{\mathrm{AH}}\, c_{\mathrm{H}^+} - k_{b2}\, c_{\mathrm{AH}_2^+}, \tag{36}$$

$$r_{\mathrm{H}^+} = -k_{a1}\, c_{\mathrm{A}^-}\, c_{\mathrm{H}^+} + k_{a2}\, c_{\mathrm{AH}} - k_{b1}\, c_{\mathrm{AH}}\, c_{\mathrm{H}^+} + k_{b2}\, c_{\mathrm{AH}_2^+}. \tag{37}$$

In Eq. (37) the water dissociation term is not included since this reaction is several orders of magnitude faster than the reactions given by Eqs. (30) and (31) (see [2]). Then, c_{OH^-} can be computed directly as

$$c_{\mathrm{OH}^-} = \frac{K_w}{c_{\mathrm{H}^+}}, \tag{38}$$

where $K_w = 10^{-8}\,\mathrm{mol}^2\,\mathrm{m}^{-6}$ is the dissociation constant for pure water at 25 °C.

Effective charge and mobility of analytes

When the concentration of the analytes is much lower than the buffer components, its effect on the pH is negligible. In such cases, considering all the ionic species involves an unnecessary high computational cost. However the influence of pH on the analytes must be taken into account. Thus the transport equation of these analytes includes $r_j = 0$, and the product $z_j \Omega_j$ as a function of pH. For example, if the species is an ampholyte that obeys a reaction scheme like the one shown in Eqs. (30) and (31), $z_j \Omega_j$ is included in Eq. (11) as an effective charge–mobility product [10]. This product is computed as $(\alpha_0 - \alpha_2)\Omega_j$, where α_0 and α_2 are the degrees of dissociation of the anionic and cationic forms, respectively. They can be written in terms of c_{H^+} as

$$\alpha_0 = \frac{\frac{K_a K_b}{c_{\mathrm{H}^+}^2}}{1 + \frac{K_b}{c_{\mathrm{H}^+}} + \frac{K_a K_b}{c_{\mathrm{H}^+}^2}}, \tag{39}$$

$$\alpha_2 = \frac{1}{1 + \frac{K_b}{c_{\mathrm{H}^+}} + \frac{K_a K_b}{c_{\mathrm{H}^+}^2}}. \tag{40}$$

Therefore the governing equation for concentration of the j-species in the sample plug is

$$\frac{\partial c_j}{\partial t} + \nabla \cdot [-(\alpha_0 - \alpha_2)\Omega_j \nabla\phi c_j + \mathbf{u} c_j - D_j \nabla c_j] = 0, \tag{41}$$

where the transport of analytes is coupled to their degree of dissociation at a given pH.

References

1. Albrecht JW, El-Ali J, Jensen KF (2007) Cascaded free-flow isoelectric focusing for improved focusing speed and resolution. Anal Chem 79:9364–9371
2. Arnaud I, Josserand J, Rossier J, Girault H (2002) Finite element simulation of off-gel buffering. Electrophoresis 23:3253–3261
3. Barz DP (2009) Comprehensive model of electrokinetic flow and migration in microchannels with conductivity gradients. Microfluid Nanofluidics 7(2):249–265
4. Bazilevs Y, Calo VM, Tezduyar TE, Hughes TJR (2007) YZβ discontinuity-capturing for advection-dominated processes with application to arterial drug delivery. Int J Numer Methods Fluids 54:593–608. doi:10.1002/fld.1484
5. Bercovici M, Lele SK, Santiago JG (2009) Open source simulation tool for electrophoretic stacking, focusing, and separation. J Chromatogr A 1216:1008–1018
6. Berli CLA (2008) Equivalent circuit modeling of electrokinetically driven analytical microsystems. Microfluid Nanofluidics 4(5):391–399
7. Berli CLA, Piaggio M, Deiber J (2003) Modeling the zeta potential of silica capillaries in relation to the background electrolyte composition. Electrophoresis 24:1587–1595
8. Brooks AN, Hughes TJR (1982) Streamline upwind/Petrov-Galerkin formulations for convection dominated flows with particular emphasis on the incompressible Navier-Stokes equations. Comput Methods Appl Mech Eng 32:199–259
9. Brunet E, Adjari A (2004) Generalized Onsager relations for electrokinetic effects in anisotropic and heterogeneous geometries. Phys Rev E 69(1):016306
10. Chatterjee A (2003) Generalized numerical formulations for multiphysics microfluidics-type applications. J Micromech Microeng 13:758–767
11. Chau M, Spiteri P, Guivarich R, Boisson H (2008) Parallel asynchronous iterations for the solution of a 3d continuous flow electrophoresis problem. Comput Fluids 37(9):1126–1137
12. Corsini A, Iossa C, Rispoli F, Tezduyar TE (2010) A DRD finite element formulation for computing turbulent reacting flows in gas turbine combustors. Comput Mech 46:159–167. doi:10.1007/s00466-009-0441-0

13. Corsini A, Menichini C, Rispoli F, Santoriello A, Tezduyar TE (2009) A multiscale finite element formulation with discontinuity capturing for turbulence models with dominant reactionlike terms. J Appl Mech 76:021211. doi:10.1115/1.3062967
14. Corsini A, Rispoli F, Santoriello A, Tezduyar TE (2006) Improved discontinuity-capturing finite element techniques for reaction effects in turbulence computation. Comput Mech 38:356–364. doi:10.1007/s00466-006-0045-x
15. Corsini A, Rispoli F, Tezduyar TE (2011) Stabilized finite element computation of NOx emission in aero-engine combustors. Int J Numer Methods Fluids 65:254–270. doi:10.1002/fld.2451
16. Corsini A, Rispoli F, Tezduyar TE (2012) Computer modeling of wave-energy air turbines with the SUPG/PSPG formulation and discontinuity-capturing technique. J Appl Mech 79:010910. doi:10.1115/1.4005060
17. Craven TJ, Rees JM, Zimmerman WB (2008) On slip velocity boundary conditions for electroosmotic flow near sharp corners. Phys Fluids 20(4):043603
18. Ermakov S, Jacobson S, Ramsey J (1998) Computer simulations of electrokinetic transport in microfabricated channel structures. Anal Chem 70(21):4494–4504
19. Ganjoo DK, Tezduyar TE (1987) Petrov-Galerkin formulations for electrochemical processes. Comput Methods Appl Mech Eng 65:61–83. doi:10.1016/0045-7825(87)90183-6
20. Ganjoo DK, Tezduyar TE, Goodrich WD (1989) A new formulation for numerical solution of electrophoresis separation processes. Comput Methods Appl Mech Eng 75:515–530. doi:10.1016/0045-7825(89)90045-5
21. Hessel V, Lowe H, Schönfeld F (2005) Micromixers—a review on passive and active mixing principles. Chem Eng Sci 60(8–9):2479–2501
22. Hruška V, Jaros M, Gaš B (2006) Simul 5—free dynamic simulator of electrophoresis. Electrophoresis 27:984–991
23. Hsu MC, Bazilevs Y, Calo VM, Tezduyar TE, Hughes TJR (2010) Improving stability of stabilized and multiscale formulations in flow simulations at small time steps. Comput Methods Appl Mech Eng 199:828–840. doi:10.1016/j.cma.2009.06.019
24. Hughes T, Mallet M (1986) A new finite element formulation for computational fluid dynamics: IV a discontinuity-capturing operator for multidimensional advective-diffusive systems. Comput Methods Appl Mech Eng 58(3):329–336
25. Hughes TJR, Franca LP, Balestra M (1986) A new finite element formulation for computational fluid dynamics: V. Circumventing the Babuška–Brezzi condition: a stable Petrov–Galerkin formulation of the Stokes problem accommodating equal-order interpolations. Comput Methods Appl Mech Eng 59:85–99
26. Hughes TJR, Mallet M, Mizukami A (1986) A new finite element formulation for computational fluid dynamics: II. Beyond SUPG. Comput Methods Appl Mech Eng 54:341–355
27. Hughes TJR, Tezduyar TE (1984) Finite element methods for first-order hyperbolic systems with particular emphasis on the compressible Euler equations. Comput Methods Appl Mech Eng 45:217–284. doi:10.1016/0045-7825(84)90157-9
28. Hunter R (2001) Foundations of colloid science, 2nd edn. Oxford University Press, Oxford
29. Karniadakis G, Beşkök A, Aluru N (2005) Microflows and nanoflows: fundamentals and simulation. Springer, New York
30. Kler P (2010) Modeling and simulation of microfluidic chips for analytical applications. Ph.D thesis, UNIVERSIDAD NACIONAL DEL LITORAL
31. Kler P, Berli C, Guarnieri F (2011) Modeling and high performance simulation of electrophoretic techniques in microfluidic chips. Microfluid Nanofluid 10(1):187–198
32. Kler PA, López EJ, Dalcín LD, Guarnieri FA, Storti MA (2009) High performance simulations of electrokinetic flow and transport in microfluidic chips. Comput Methods Appl Mech Eng 198(30–32):2360–2367
33. Li D (2004) Electrokinetics in microfluidics. Elsevier Academic Press, London
34. MacInnes JM (2002) Computation of reacting electrokinetic flow in microchannel geometries. Chem Eng Sci 57(21):4539–4558
35. Park YJ, Deans HA, Tezduyar TE (1990) Finite element formulation for transport equations in a mixed coordinate system: an application to determine temperature effects on the single-well chemical tracer test. Int J Numer Methods Fluids 11:769–790. doi:10.1002/fld.1650110605
36. Park YJ, Deans HA, Tezduyar TE (1991) Thermal effects on single-well chemical tracer tests for measuring residual oil saturation. Soc Petroleum Eng Form Eval 190:401–408. doi:10.2118/19683-PA
37. Patankar N, Hu H (1998) Numerical simulation of electroosmotic flow. Anal Chem 70(9):1870–1881
38. Peng Y, Pallandre A, Tran NT, Taverna M (2008) Recent innovations in protein separation on microchips by electrophoretic methods. Electrophoresis 29(1):157–178
39. Probstein R (2003) Physicochemical hydrodynamics. An Introduction, 2nd edn. Wiley-Interscience, New York
40. Rispoli F, Corsini A, Tezduyar TE (2007) Finite element computation of turbulent flows with the discontinuity-capturing directional dissipation (DCDD). Comput Fluids 36:121–126. doi:10.1016/j.compfluid.2005.07.004
41. Rispoli F, Saavedra R, Corsini A, Tezduyar TE (2007) Computation of inviscid compressible flows with the V-SGS stabilization and YZβ shock-capturing. Int J Numer Methods Fluids 54:695–706. doi:10.1002/fld.1447
42. Rispoli F, Saavedra R, Menichini F, Tezduyar TE (2009) Computation of inviscid supersonic flows around cylinders and spheres with the V-SGS stabilization and YZβ shock-capturing. J Appl Mech 76:021209. doi:10.1115/1.3057496
43. Saville D, Palusinski O (1986) Theory of electrophoretic separations. Part I: formulation of a mathematical model. AIChE J 32(2):207–214
44. Schönfeld F, Hessel V, Hofmann C (2004) An optimised split-and-recombine micro-mixer with uniform 'chaotic' mixing. Lab Chip 4(1):65–69
45. Shim J, Dutta P, Ivory C (2007) Modeling and simulation of IEF in 2-D microgeometries. Electrophoresis 28:572–586
46. Sounart TL, Baygents JC (2007) Lubrication theory for electroosmotic flow in a non-uniform electrolyte. J Fluid Mech 576:139–172
47. Takizawa K, Tezduyar TE (2011) Multiscale space–time fluid–structure interaction techniques. Comput Mech 48:247–267. doi:10.1007/s00466-011-0571-z
48. Tezduyar TE (1992) Stabilized finite element formulations for incompressible flow computations. Adv Appl Mech 28:1–44. doi:10.1016/S0065-2156(08)70153-4
49. Tezduyar TE (2003) Computation of moving boundaries and interfaces and stabilization parameters. Int J Numer Methods Fluids 43:555–575. doi:10.1002/fld.505
50. Tezduyar TE (2004) Finite element methods for fluid dynamics with moving boundaries and interfaces. In: Stein E, Borst RD, Hughes TJR (eds) Encyclopedia of computational mechanics, vol 3: Fluids, chap. 17. Wiley, New York
51. Tezduyar TE, Behr M, Liou J (1992) A new strategy for finite element computations involving moving boundaries and interfaces—the deforming-spatial-domain/space–time procedure: I. The concept and the preliminary numerical tests. Comput Methods Appl Mech Eng 94(3):339–351. doi:10.1016/0045-7825(92)90059-S
52. Tezduyar TE, Behr M, Mittal S, Liou J (1992) A new strategy for finite element computations involving moving boundaries

and interfaces – the deforming-spatial-domain/space–time procedure: II. Computation of free-surface flows, two-liquid flows, and flows with drifting cylinders. Comput Methods Appl Mech Eng 94(3):353–371. doi:10.1016/0045-7825(92)90060-W
53. Tezduyar TE, Mittal S, Ray SE, Shih R (1992) Incompressible flow computations with stabilized bilinear and linear equal-order-interpolation velocity-pressure elements. Comput Methods Appl Mech Eng 95:221–242. doi:10.1016/0045-7825(92)90141-6
54. Tezduyar TE, Osawa Y (2000) Finite element stabilization parameters computed from element matrices and vectors. Comput Methods Appl Mech Eng 190:411–430. doi:10.1016/S0045-7825(00)00211-5
55. Tezduyar TE, Park YJ (1986) Discontinuity capturing finite element formulations for nonlinear convection-diffusion-reaction equations. Comput Methods Appl Mech Eng 59:307–325. doi:10.1016/0045-7825(86)90003-4
56. Tezduyar TE, Park YJ, Deans HA (1987) Finite element procedures for time-dependent convection-diffusion-reaction systems. Int J Numer Methods Fluids 7:1013–1033. doi:10.1002/fld.1650071003
57. Tezduyar TE, Ramakrishnan S, Sathe S (2008) Stabilized formulations for incompressible flows with thermal coupling. Int J Numer Methods Fluids 57:1189–1209. doi:10.1002/fld.1743
58. Tezduyar TE, Sathe S (2007) Modeling of fluid–structure interactions with the space–time finite elements: solution techniques. Int J Numer Methods Fluids 54:855–900. doi:10.1002/fld.1430
59. Tezduyar TE, Senga M (2006) Stabilization and shock-capturing parameters in SUPG formulation of compressible flows. Comput Methods Appl Mech Eng 195:1621–1632. doi:10.1016/j.cma.2005.05.032
60. Tezduyar TE, Senga M (2007) SUPG finite element computation of inviscid supersonic flows with YZβ shock-capturing. Comput Fluids 36:147–159. doi:10.1016/j.compfluid.2005.07.009
61. Tezduyar TE, Senga M, Vicker D (2006) Computation of inviscid supersonic flows around cylinders and spheres with the SUPG formulation and YZβ shock-capturing. Comput Mech 38:469–481. doi:10.1007/s00466-005-0025-6
62. Thormann W, Caslavska J, Mosher R (2007) Modeling of electroosmotic and electrophoretic mobilization in capillary and microchip isoelectric focusing. J Chromatogr A 1155(2):154–163
63. Tsai WB, Hsieh CJ, Chieng CC (2005) Parallel computation of electroosmotic flow in L-shaped microchannels. In: 6th world congress of structural and multidisciplinary optimization, pp 4971–4980
64. Wu D, Qin J, Lin B (2008) Electrophoretic separations on microfluidic chips. J Chromatogr A 1184(1–2):542–559